Mechanics of Materials 41 (2009) 495–505

Contents lists available at ScienceDirect

Mechanics of Materials

journal homepage: www.elsevier.com/locate/mechmat

New approach to the computation of the form factor of viscoelastic cylinders

Basel M. Seoudi [a], Victor M. Kulik [b], Andrey V. Boiko [c], H.H. Chun [d], Inwon Lee [d,*]

[a] Department of Marine Engineering Technology, Arab Academy for Science, Technology and Maritime Transport, Alexandria, PO Box 1029, Egypt
[b] Institute of Thermophysics, Russian Academy of Sciences, Novosibirsk 630058, Russia
[c] Institute of Theoretical and Applied Mechanics, Russian Academy of Sciences, Novosibirsk 630090, Russia
[d] Advanced Ship Engineering Research Center (ASERC), Pusan National University, San 30, Jangjeon-dong, Geumjeong-gu, Busan 609-735, Republic of Korea

ARTICLE INFO

Article history:
Received 10 September 2007
Received in revised form 28 November 2008

ABSTRACT

Periodic deformations of the viscoelastic elastomers were investigated numerically by solving the two-dimensional elastic wave equations. In order to enhance the accuracy of the viscoelastic material property calculations, a pseudospectral analysis method was employed. This allowed us to exclude the use of the dynamic form factor derived from the conventional 1D model. Based on the present 2D method, the validity of the conventional 1D form factor concept was evaluated. The present 2D method was used to calculate the vibration response of the elastomer samples under harmonic excitation. Obtained numerical results were compared with those using the simplest 1D model. Valid range of the form factor was examined. Empirical formulas to correct static and dynamic form factors for both normal deformation mode and the shear deformation mode, which are suitable for engineering applications, are suggested.

1. Introduction

Viscoelastic properties of polymeric materials are required in various scientific and engineering applications such as polymer science (Ferry, 1961; Riande et al., 2000), attenuation of sound and vibration (Tsai and Hsueh, 2001) and skin friction reduction using compliant coating (Kulik et al., 2005). For relatively slow processes with characteristic frequencies less than 1 Hz, the materials are characterized usually in terms of relaxation time, which describe a transient response to the excitations on the sample. For faster processes it is convenient to express the such viscoelastic properties as the elasticity modulus E, the loss tangent μ and the Poisson's ratio σ as functions of frequency.

The elasticity modulus of rubber-like materials varies in wide range from 10^4 to 10^7 Pa. The loss tangent is defined as a phase lag of material deformation to an applied periodic load ($\mu = \tan\theta = \mathrm{Im}E^*/\mathrm{Re}E^*$), where E^* is a complex modules of elasticity. The rate between the energy dissipated during one period of deformation to maximum potential energy of the deformed material directly depends on the loss tangent. The loss tangent is close to zero for inviscid (purely elastic) materials, but it can reach quite large value about 0.5–1 under viscous effect. Additional significant parameter is the Poisson's ratio σ, which is the ratio of the lateral contraction to the elongation in an infinitesimally small uniaxial extension.

There are so many techniques to measure viscoelastic properties of isotropic materials in frequency range 20–200 Hz. This range is characteristic for noise and vibrations of industrial facilities. The techniques for the frequency range from 200 to 10 kHz was reported by several authors (Chen and Lakes, 1989; Fitzgerald and Ferry, 1953; Madigosky and Lee, 1983). Most reported methods have drawbacks, i.e., complicated apparatus which is not easily applicable in real practice or limited geometry. As an alternative, method based on temperature-frequency analogy of Williams–Landel–Ferry was proposed (Ferry, 1961), which convert the temperature dependence of E and μ measured at resonance frequency to the frequency dependence at a

* Corresponding author. Tel.: +82 51 510 2764; fax: +82 51 581 3718.
E-mail address: inwon@pusan.ac.kr (I. Lee).

0167-6636/$ - see front matter © 2009 Elsevier Ltd. All rights reserved.
doi:10.1016/j.mechmat.2009.01.026

fixed temperature. However, this method has essential drawbacks, because not all materials obey this rule, furthermore, the conversion factors are *a priori* unknown. Recently, relatively simple methods have been proposed by Smith et al. (1983) and Kulik and Semenov (1986) for wide frequency band. The measuring frequency range depends mainly on the loading mass and sensitivity of accelerometers that used to document the response of the mechanical system subjected to the dynamic test. However, this technique requires the use of a form factor, which depends primarily on the geometrical shape of the samples (Chen and Lakes, 1989; Riande et al., 2000). For example, let us consider linear stationary deformation, in which case, the measured effective elasticity modulus is described by Hook's law

$$E_{\text{eff}} = \frac{F/S}{\Delta H/H} \tag{1}$$

where F is the applied force, $S = \pi R^2$ and H are the area and the height of the sample, respectively, and ΔH is the height change under the applied force. As the ratio H/R increases, E_{eff} tends asymptotically to a constant value E. The ratio $\alpha_E = E/E_{\text{eff}}$ is called a form factor. Similarly, in the case of unsteady loading, one can introduce a form factor α_μ to correct the measured loss tangent $\alpha_\mu = \mu/\mu_{\text{eff}}$. The values of α_E and α_μ depend on the Poisson's ratio σ, and some other sample characteristics. All dependencies are unknown *a priori* and have to be estimated for various sample shapes under tests.

In the present study, an assessment of the form factor concept has been performed. Toward this end, a series of numerical test has been attempted based on the numerical analysis for a two-dimensional elastic wave equation. The numerical techniques for deformed states are well developed and summarized, for example, in Sadd (2005) and Timoshenko and Groodier (1982). Certain difficulties appear in boundary conditions, which can be incompatible to each other in corner points both under static and dynamic loads. For large static deformations, Tsai (2005) assumed a parabolic barreling of a sample bonded between two rigid plates, which makes it possible to estimate the form factor without complicated calculations. The barrel shape and the form factor were found by Rosin (1972) based on variational principles. However, under dynamic forcing, the sample can change its shape in more complicated manner. In this study, a technique for numerical calculation of the elasticity modulus E and the loss tangent μ as well as the correction factors for the form factors derived from 1D analysis for two practically important setups.

2. Two-dimensional dynamic deformations of bonded samples

2.1. Governing equations

Fig. 1 illustrates two kinds of viscoelastic sample shapes under considerations, a circular cylinder with the radius R and an annulus with the inner and the outer radii being R_0 and R_1. The former is to undergo tensile ocillatory deformation while the latter corresponds to shear mode. The axial length and the mass of the sample are H and m. The samples consist of the viscoelastic material with the modulus of elasticity E, loss tangent μ and Poisson's ratio σ. The samples are attached to the oscillating table on one side and loaded with a mass M on the other side. The oscillating table excites a harmonic oscillation with amplitude A_0 and frequency ω. The load mass M attached on the other side of the sample exhibits the same frequency of oscillation with the amplitude ZA_0 and the phase lag θ.

The displacement of the particle in the axisymmetric sample shapes due to the wave can be described as

$$\vec{\xi} = \zeta(r,z)\hat{e}_z + \eta(r,z)\hat{e}_r,$$

where the radial displacement $\eta(r,z)$ is an odd function and axial displacement $\zeta(r,z)$ is an even function of r. The stress-strain relations are the form

$$\sigma_{rr} = \frac{E\sigma}{(1-2\sigma)(1+\sigma)}\left(\frac{\partial\eta}{\partial r} + \frac{\eta}{r} + \frac{\partial\zeta}{\partial z}\right) + \frac{E}{1+\sigma}\frac{\partial\eta}{\partial r}$$

$$\sigma_{zz} = \frac{E\sigma}{(1-2\sigma)(1+\sigma)}\left(\frac{\partial\eta}{\partial r} + \frac{\eta}{r} + \frac{\partial\zeta}{\partial z}\right) + \frac{E}{1+\sigma}\frac{\partial\zeta}{\partial z}$$

$$\sigma_{zr} = \frac{E\sigma}{2(1+\sigma)}\left(\frac{\partial\eta}{\partial z} + \frac{\partial\zeta}{\partial r}\right)$$

The governing equation for two dimensional elastic wave in isotropic medium (Landau and Lifschitz, 1986) takes the form

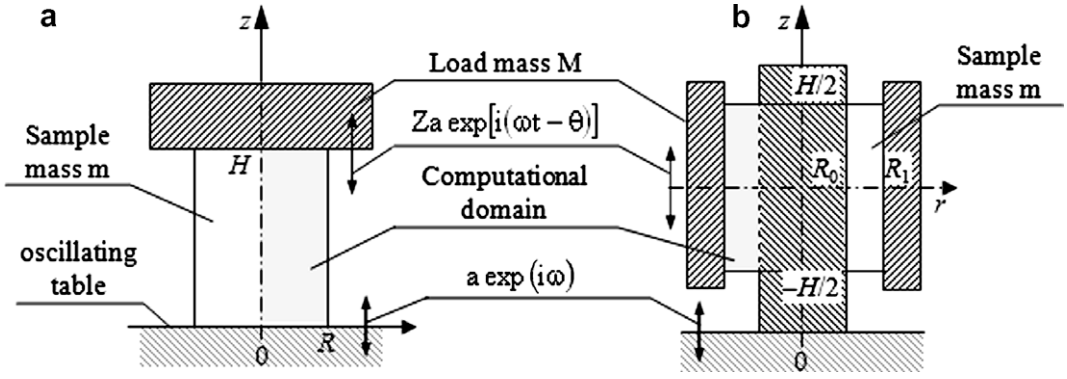

Fig. 1. Schematic diagram of sample; (a) normal deformation mode, (b) shear deformation mode.

$$\frac{\partial^2 \vec{\xi}}{\partial t^2} = C_t^2 \Delta \vec{\xi} + (C_\ell^2 - C_t^2)\nabla(\nabla \cdot \vec{\xi}), \tag{2}$$

where $C_t^2 = \frac{E(1+i\mu)}{2\rho(1+\sigma)}$, $C_\ell^2 = \frac{E(1+i\mu)(1-\sigma)}{\rho(1+\sigma)(1-2\sigma)}$, $\rho = \frac{m}{\pi R^2 H}$.

If harmonic excitation is assumed, then Eq. (2) can be written as

$$\begin{aligned} &C_l^2\left(r\frac{\partial \eta}{\partial r} - \eta + r^2\frac{\partial^2 \eta}{\partial r^2} + r^2\frac{\partial^2 \zeta}{\partial r \partial z}\right) + C_t^2 r^2\left(\frac{\partial^2 \eta}{\partial z^2} - \frac{\partial^2 \zeta}{\partial r \partial z} + \frac{\eta}{r^2}\right) \\ &\quad + r^2\omega^2\eta = 0, \\ &C_l^2\left(r\frac{\partial^2 \eta}{\partial r \partial z} + \frac{\partial \eta}{\partial z} + r\frac{\partial^2 \zeta}{\partial z^2}\right) + C_t^2\left(\frac{\partial \zeta}{\partial r} - \frac{\partial \eta}{\partial z} + r\frac{\partial^2 \zeta}{\partial r^2} - r\frac{\partial^2 \eta}{\partial r \partial z}\right) \\ &\quad + r\omega^2\zeta = 0. \end{aligned} \tag{3}$$

2.2. Boundary conditions for the cylindrical sample

The boundary conditions for the cylindrical sample (normal strain mode) can be written as:

(a) Absence of radial displacements at bonded surfaces

$$\eta = 0 \text{ at } z = 0, \tag{4}$$
$$\eta = 0 \text{ at } z = H, \tag{5}$$

(b) Axial harmonic displacements at the lower and upper surfaces

$$\zeta = A_0 e^{i\omega t} \text{ at } z = 0, \tag{6}$$
$$\zeta = ZA_0 e^{i(\omega t - \theta)} \text{ at } z = H, \tag{7}$$

(c) Absence of strains at the side surface (at $r = R$)

$$\sigma_{rz} = 0 \to \frac{\partial \eta}{\partial z} + \frac{\partial \zeta}{\partial r} = 0, \tag{8}$$
$$\sigma_{rr} = 0 \to (1-\sigma)\frac{\partial \eta}{\partial r} + \sigma\left(\frac{\partial \zeta}{\partial z} + \frac{\eta}{r}\right) = 0, \tag{9}$$

Additionally, symmetry conditions can be used along the cylinder axis:

$$\eta(r = 0) = 0, \quad \frac{\partial \zeta}{\partial r}(r = 0) = 0.$$

The procedure to obtain E and μ is to solve an inverse problem defined by Eqs. (3)–(9). Toward this end, measured data of the oscillation magnitude ratio Z and the phase delay θ are utilized. Unique solution is obtained with the help of the following compatibility condition

$$\begin{aligned} M\frac{\partial^2 \zeta}{\partial t^2} &= -2\pi\rho C_\ell^2 \int_0^R \sigma_{zz}(H, r) r \mathrm{d}r \to MZ\omega^2 e^{i(\omega t - \theta)} \\ &= 2\pi\frac{E(1+i\mu)(1-\sigma)}{(1+\sigma)(1-2\sigma)} \int_0^R \frac{\partial \zeta}{\partial z}(H, r) r \mathrm{d}r, \end{aligned} \tag{10}$$

which equates internal stress at the upper edge with the pressure developed by the movement of the finite load mass M.

2.3. Boundary conditions for the annular sample

The boundary conditions for the ring sample (shear strain mode) are as follows:

(a) Absence of radial displacements at bonded surfaces

$$\eta = 0 \text{ at } r = R_0, \tag{11}$$
$$\eta = 0 \text{ at } r = R_1, \tag{12}$$

(b) Axial harmonic displacements at both radii

$$\zeta = A_0 e^{i\omega t} \text{ at } r = R_0, \tag{13}$$
$$\zeta = ZA_0 e^{i(\omega t - \theta)} \text{ at } r = R_1, \tag{14}$$

(c) Absence of strains at the upper and lower surfaces (at $z = -H/2$ and $z = H/2$)

$$\sigma_{rz} = 0 \to \frac{\partial \eta}{\partial z} + \frac{\partial \zeta}{\partial r} = 0, \tag{15}$$
$$\sigma_{zz} = 0 \to (1-\sigma)\frac{\partial \zeta}{\partial z} + \sigma\left(\frac{\partial \eta}{\partial r} + \frac{\eta}{r}\right) = 0, \tag{16}$$

Similarly with Eq. (10), the compatibility requires that the stress at the outer edge ($r = R_1$) be equal to the pressure developed by the movement of the finite load mass M,

$$\begin{aligned} M\frac{\partial^2 \zeta}{\partial t^2} &= -4\pi R_1 \rho C_t^2 \int_0^{H/2} \sigma_{rr}(z, R_1) \mathrm{d}z \to MZ\omega^2 e^{i(\omega t - \theta)} \\ &= \frac{2\pi R_1 E(1+i\mu)}{1+\sigma} \int_0^{H/2} \frac{\partial \zeta}{\partial r}(z, R_1) \mathrm{d}z. \end{aligned} \tag{17}$$

2.4. One-dimensional model equations

Apart from the two-dimensional wave equation in the above, one-dimensional variant needs to be analyzed separately because the major goal of the present study is to estimate the form factor based on the one-dimensional model. In this one-dimensional analysis, the radial deformation component is neglected and the governing equation regarding the axial deformation is solved to get E_{eff} and μ_{eff} as in Kulik and Semenov (1986).

The governing equation for the cylindrical sample in Fig. 1a is given as

$$\rho\frac{\partial^2 \zeta(y,t)}{\partial t^2} = E_{\text{eff}}(1 + i\mu_{\text{eff}})\frac{\partial^2 \zeta(y,t)}{\partial z^2}, \tag{18}$$

with the boundary conditions of Eqs. (6) and (7) and the following compatibility condition

$$\frac{M}{S}\frac{\partial^2 \zeta}{\partial t^2} = -E_{\text{eff}}(1 + i\mu_{\text{eff}})\frac{\partial \zeta(y,t)}{\partial z} \text{ at } z = H. \tag{19}$$

On the other hand, for the annular sample in Fig. 1b, the corresponding equations becomes

$$\rho\frac{\partial^2 \zeta(y,t)}{\partial t^2} = G_{\text{eff}}(1 + i\mu_{\text{eff}})\frac{\partial^2 \zeta(y,t)}{\partial r^2}, \tag{20}$$

with the boundary conditions of Eqs. (13) and (14) the following compatibility condition

$$\frac{M}{S}\frac{\partial^2 \zeta}{\partial t^2} = -G_{\text{eff}}(1 + i\mu_{\text{eff}})\frac{\partial \zeta(y,t)}{\partial r} \text{ at } r = R_1, \tag{21}$$

where G_{eff} is effective shear modulus. Further reductions of $E_{\text{eff}}(f)$, $G_{\text{eff}}(f)$ and $\mu_{\text{eff}}(f)$ to obtain a correction for the form factor applicable for a variety of E and μ are described in Section 3.

2.5. Solution procedure

Without loss of generality, the solution technique for the two-dimensional wave equation is described for the Eqs. (3)–(9) in case of the cylindrical sample. To solve them numerically, a pseudospectral approximation of the wave equations with $N_z \times N_r$ mesh points was used (Canuto et al., 1988). A grid was set up based on Chebyshev Gauss–Lobatto knots independently in z and r, thereby producing so-called tensor product grid. Let the rows and columns of the $(N+1) \times (N+1)$ Chebyshev spectral differentiation matrix D_N be indexed from 0 to N. The entries of this matrix are given by the following rules (Canuto et al., 1988; Trefethen, 1990)

$$(D_N)_{00} = \frac{2N^2+1}{6}, \quad (D_N)_{NN} = -(D_N)_{00},$$
$$(D_N)_{jj} = \frac{-x_j}{2(1-x_j^2)}, \quad j = 1, \ldots N-1,$$
$$(D_N)_{ij} = \frac{c_i}{c_j}\frac{(-1)^{i+j}}{x_i - x_j}, \quad i \neq j, i, j = 1, \ldots N-1,$$

where $x_k = \cos(k\pi/N), k = 0, 1, \cdots, N$ and

$$c_i = \begin{cases} 2 & i = 0 \text{ or } N \\ 1 & \text{otherwise} \end{cases}$$

Due to the incompatibility of the boundary conditions in the corner points at $r = R,\ z = 0,$ and $r = R,\ z = H$, where $\partial\zeta/\partial z$ and $\partial\zeta/\partial r$ can be discontinuous, the accuracy of the calculation of the integrals in Eqs. (10) and (17) is relatively low (Grinchenko and Meleshko, 1981). However, the corner singularities in these cases are quite weak and a reduction of the error to an admissible value can be achieved, e.g., by an appropriate coordinate transformation, which condense the knots at the corners (Tang and Trummer, 1996). Toward this end, the following coordinate transformation was employed:

$$y = \frac{\arctan(ax)}{\arctan(a)},$$

which mapped the polynomial domain $[-1;1] \times [-1;1]$ onto itself. In the numerical tests described in the next section $a = 2$ was used.

Then, a linear coordinate transformation mapped the problem from the polynomial domain $[-1;1] \times [-1;1]$ to the physical domain $[0;H] \times [-R;R]$. Specifically, we consider the mesh $(r_i, z_j), r_i = R\cos\left(\frac{i\pi}{N_r}\right), z_j = \frac{H}{2}\left[\cos\left(\frac{j\pi}{N_r}\right)+1\right]$, $i = 0, \cdots, N_r, j = 0, \cdots, N_r$. Let us represent the functions of displacements $\eta(r_i,z_j)$ and $\zeta(r_i,z_j)$ in the mesh points by the matrices $(\eta)_{i,j}$ and $(\zeta)_{i,j}$ and denote the first discrete derivative operators in r and z as $\bar{D}_r = D_{N_r}/R$ and $\bar{D}_z = 2D_{N_z}/H$, respectively. For the sake of simplicity, odd integers for N_r were used in these calculations. Then, due to the axial symmetry of the problem under consideration, we are interested only in the solution at $r \in [0;R]$, in which case the matrix $\bar{D}_r$ can be reduced to the matrices $\bar{\bar{D}}_r$ for the even function $\zeta(r_i,z_j)$ and $\tilde{\bar{D}}_r$ for the odd function $\eta(r_i,z_j)$, of which elements are given as

$$(\bar{\bar{D}}_r)_{ij} = (\bar{D}_r)_{ij} + (\bar{D}_r)_{ik}, i, j = 0 \ldots (N+1)/2, k = N+1-j$$
$$(\tilde{\bar{D}}_r)_{ij} = (\bar{D}_r)_{ij} - (\bar{D}_r)_{ik}, i, j = 0 \ldots (N+1)/2, k = N+1-j$$

If we reassemble the matrices η and ζ into the column vectors built by the columns of η and ζ written one by one (that is we represent them in the lexicographic order), the directional derivative matrices may be expressed as tensorial (Kroneker) products and become (Trefethen, 1990)

$$\bar{D}_r = \bar{\bar{D}}_r \otimes I_z, \tilde{D}_r = \tilde{\bar{D}}_r \otimes I_z,$$
$$D_z = I_r \otimes \bar{D}_z,$$
$$\bar{D}_{rr} = \bar{\bar{D}}_r^2 \otimes I_z, \tilde{D}_{rr} = \tilde{\bar{D}}_r^2 \otimes I_z,$$
$$D_{zz} = I_r \otimes \bar{D}_z^2,$$
$$\bar{D}_{rz} = \bar{\bar{D}}_r \otimes \bar{D}_z, \tilde{D}_{rz} = \tilde{\bar{D}}_r \otimes \bar{D}_z,$$

where I_z and I_r are the unit (N_z+1) and (N_r+1) matrices, respectively. Then, the original system of equations is approximated by the following matrix equation

$$\begin{bmatrix} C_\ell^2(r^2\tilde{D}_{rr} + r\tilde{D}_r - I_r \otimes I_z) + C_t^2 r^2 D_{zz} + r^2\omega^2 & (C_\ell^2 - C_t^2) r^2 \bar{D}_{rz} \\ (C_\ell^2 - C_t^2)(r\tilde{D}_{rz} + D_z) & C_t^2(r\bar{D}_{rr} + \bar{D}_r) + C_\ell^2 r D_{zz} + r\omega^2 \end{bmatrix} \times \begin{pmatrix} \eta \\ \zeta \end{pmatrix} = 0.$$

Boundary conditions were applied explicitly by changing the corresponding rows in the left and right-hand sides of the equations (Trefethen, 1990) to make inhomogeneous problems, which are then easily solved by the left matrix division. Final approximations of E and μ were obtained by Gauss-Newton iterations of the obtained solutions to satisfy the compatibility condition, Eq. (10).

For the shear mode deformation, solution of Eqs. (3), (11)–(17) are obtained similarly. It was found that as the number of knots in each direction is increased from 12 to 20, the approximated values of E and μ change less than 1% in the region of interest within estimated experimental error in measuring the amplitudes and phase shifts of the axial displacement (see details of real experimental setup and measurements in Kulik et al., 2008). The calculations were performed in MATLAB.

The solution of Eq. (18) with the boundary conditions Eqs. (6), (7), and (19) or equivalently, Eq. (20) with the boundary conditions Eqs. (13), (14), and (21) can be found in an implicit form analytically (Kulik and Semenov, 1986; Kulik et al., 2007). Let us consider for brevity only the first case and assume the solution to be in the following form

$$\zeta = F(z)e^{i\omega t}.$$

Substituting ζ in Eq. (2) gives an ordinary differential equation

$$-\omega^2\rho F(z) = E_{\text{eff}}(1 + i\mu_{\text{eff}})\frac{d^2F}{dz^2}, \tag{22}$$

of which the solution can be written as

$$F(y) = C_1 e^{i\delta z} + C_2 e^{-i\delta z}, \tag{23}$$

where

$$\delta = \omega\sqrt{\frac{\rho}{E_{\text{eff}}(1+i\mu_{\text{eff}})}} = \omega\sqrt{\frac{\rho}{E_{\text{eff}}}}\left[\sqrt{\frac{\sqrt{1+\mu_{\text{eff}}^2}-1}{2(1+\mu_{\text{eff}}^2)}} + i\sqrt{\frac{\sqrt{1}+\mu_{\text{eff}}^2+1}{2(1+\mu_{\text{eff}}^2)}}\right]. \tag{24}$$

Application of the boundary condition of Eq. (6) leads to

$$C_1 + C_2 = a. \tag{25}$$

From the boundary condition Eq. (12), the following equation is obtained

$$-\frac{M}{S}\omega^2(C_1 e^{i\delta H} + C_2 e^{-i\delta H}) = C_1\delta e^{i\delta H} - C_2\delta e^{-i\delta H}. \tag{26}$$

Constants C_1 and C_2 can be obtained by solving Eqs. (25) and (26). Substituting C_1 and C_2 into Eqs. (22) and (23) and equating $z = H$ gives the displacement of the load mass, which is in the form of $\zeta(H) = Zae^{i(\omega t-\theta)}$. By arranging the terms, the following equation is obtained:

$$\frac{e^{i\theta}}{Z} = \cos(\delta H) - \frac{M\omega^2}{S\delta E_{\text{eff}}(1+i\mu_{\text{eff}})}\sin(\delta H). \tag{27}$$

In order to make Eqs. (22) and (27) dimensionless, the parameters

$$C = \sqrt{\frac{\rho\omega^2 H^2}{E_{\text{eff}}(1+i\mu_{\text{eff}})}},\quad m = \rho\pi R^2 H.$$

are employed. This yields an implicit equation:

$$\frac{e^{i\theta}}{Z} = \cos(C) - iC\frac{M}{m}\sin(C). \tag{28}$$

which can be further reduced to

$$Z\sqrt{1+\left(C\frac{M}{m}\right)^2}\exp\left[C + i\tan^{-1}\left(C\frac{M}{m}\right) - i\theta\right] = 1. \tag{29}$$

Taking natural logarithm of both sides yields

$$\frac{1}{2}\ln\left[Z^2 + \left(\frac{ZCM}{m}\right)^2\right] + C + i\tan^{-1}\left(C\frac{M}{m}\right) - i\theta = 0. \tag{30}$$

Then, a solution of Eq. (30) with respect to complex variable C is easily obtained by a nonlinear equation solver. Equations of 1D model of deformation were solved using such algorithms of MATLAB as Levenberg-Marquardt and Gauss Newton, both with either mixed quadratic and cubic or only cubic polynomial interpolation and extrapolation line search methods (Fletcher, 1980).

3. Results and discussion

3.1. Displacement diagrams

Before proceeding to the estimation of form factor, it is worthwhile to examine two dimensional wave deformation behaviors. Fig. 2 illustrates typical examples of $Z(f)$ and $\theta(f)$ with varying loads mass M from the numerical test for the normal deformation mode (cylindrical sample) of Fig. 1a. The calculations were carried out in a wide frequency range including both the parametric resonance

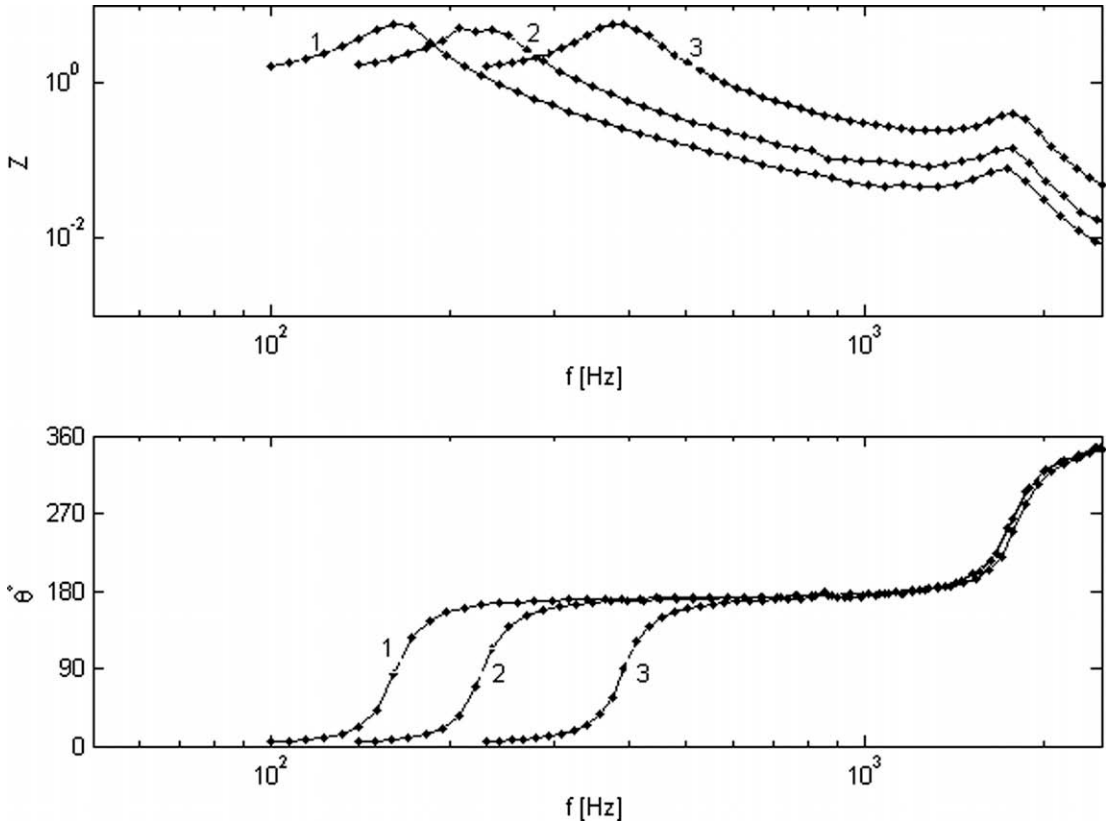

Fig. 2. Response characteristics for a cylindrical sample (R = 10 mm, H = 20 mm) with varying load mass; (1) M = 2 m, (2) M = m, and (3) M = 0.5 m, Viscoelastic material properties ρ = 1000 kg/m^3, E = 1 MPa, μ = 0.1 and σ = 0.495.

frequency $f_{par} \approx \frac{1}{H}\sqrt{\frac{E}{\rho}\frac{m}{M}}$ (Smith et al., 1983) and the fundamental resonance frequency $f_{fund} \approx \frac{1}{2H}\sqrt{\frac{E}{\rho}}$. The former depends on the load mass M while the latter does not. As the frequency passes each resonance frequency, the phase experiences a gradual shift of 180°. The phase behavior in the vicinity of the parametric resonance depends significantly on M, but at higher frequencies is essentially independent of it.

The displacements can be separated by amplitude and phase factors as

$$\eta = \eta_0(r,z)\exp\left[i\omega t + \phi_\eta(r,z)\right],$$
$$\zeta = \zeta_0(r,z)\exp\left[i\omega t + \phi_\zeta(r,z)\right]. \quad (31)$$

Corresponding diagrams of displacement amplitudes and phases for the case with $M = 5.41$ g are shown in Figs. 3 and 4 for frequencies f_{par} and f_{fund}, respectively. In both cases in accordance with the boundary conditions, the radial displacement is absent along the axis of the cylinder ($r = 0$) and at lower and upper edges. At parametric resonance (Fig. 3), the radial displacement shows barrel-like shape reaching maximum value about $\eta_{0,max} \approx 4a$ in the middle of H at the cylinder side surface. The phase of the radial displacement is independent of r and z and equal to 90°. The axial displacement grows monotonously from the lower to upper surface reaching $\zeta_{0,max} \approx 11a$. Amplitudes and phases of ζ are virtually independent of r. Upper part of the sample oscillates with 90° lag with respect to the lower part of the sample.

For the fundamental resonance in Fig. 4, the radial displacement shows two humps, whose amplitudes reach maximums at the outer surface. The displacements at the humps oscillate in antiphase indicating the presence of a standing wave. Axial displacement reaches maximum approximately at $z = H/2$ along the centerline of the sample. Its phase experience abrupt jumps at $z \approx 0$ and $z \approx H$.

General conclusion which can be drawn from Figs. 3 and 4 is that there should be a limit of quasistationary consideration of the sample barreling in the sense of works (Sadd, 2005; Timoshenko and Groodier, 1982) somewhere between the frequencies f_{par} and f_{fund}. Above this limit, there hardly exists a way to introduce a more or less universal form factor which is useful for engineering applications. In what follows we outline this frequency limit and will offer a frequency correction for $f < f_{fund}$ or $\theta < 140°$.

3.2. Form factor frequency correction

In the present study, the form factor was calculated using the procedure in Eq. (32). For E, μ and other parameters are assumed to be independent of frequency as shown in Tables 1 and 2. The dependencies $Z(f)$ and $\theta(f)$ were calculated using two-dimensional model described in Sections 2.1–2.3. Then, the estimation $E_{eff}(f)$ and $\mu_{eff}(f)$ corresponding to $Z(f)$, $\theta(f)$ and sample parameters were calculated back using one-dimensional inverse problem in Section 2.4.

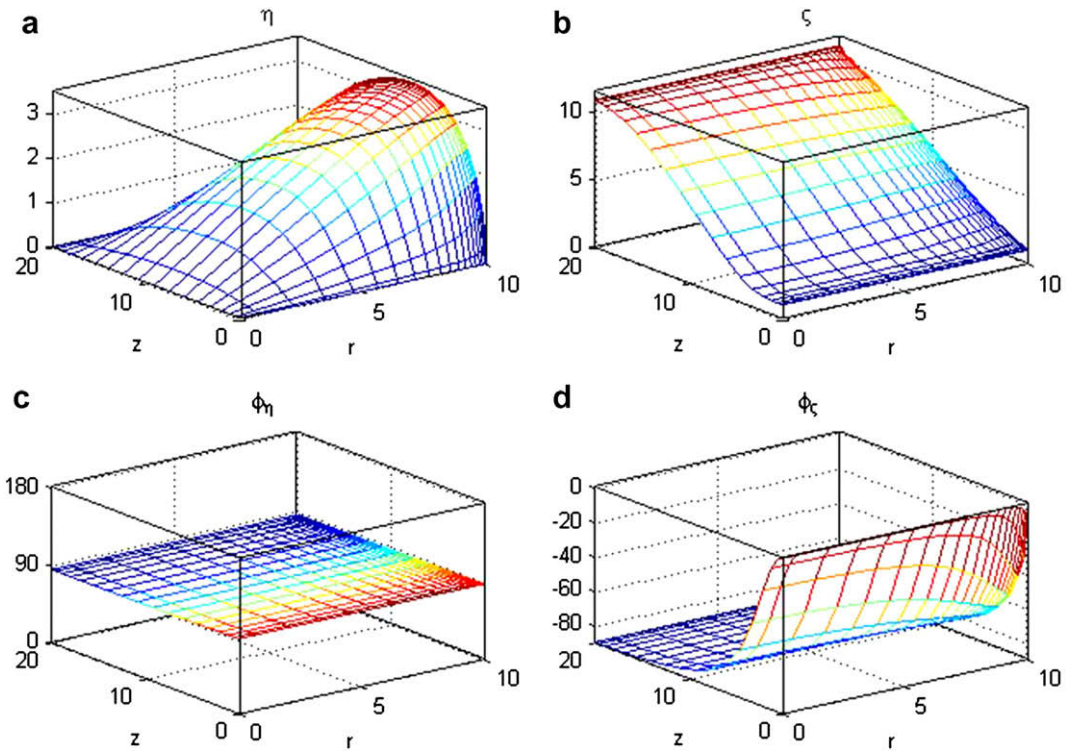

Fig. 3. Distribution of 2D deformation wave at parametric resonance frequency $f = f_{par}$; (a) amplitude of radial deformation η_0, (b) amplitude of axial deformation ζ_0, (c) phase of radial deformation φ_η, (d) phase of axial deformation φ_ζ.

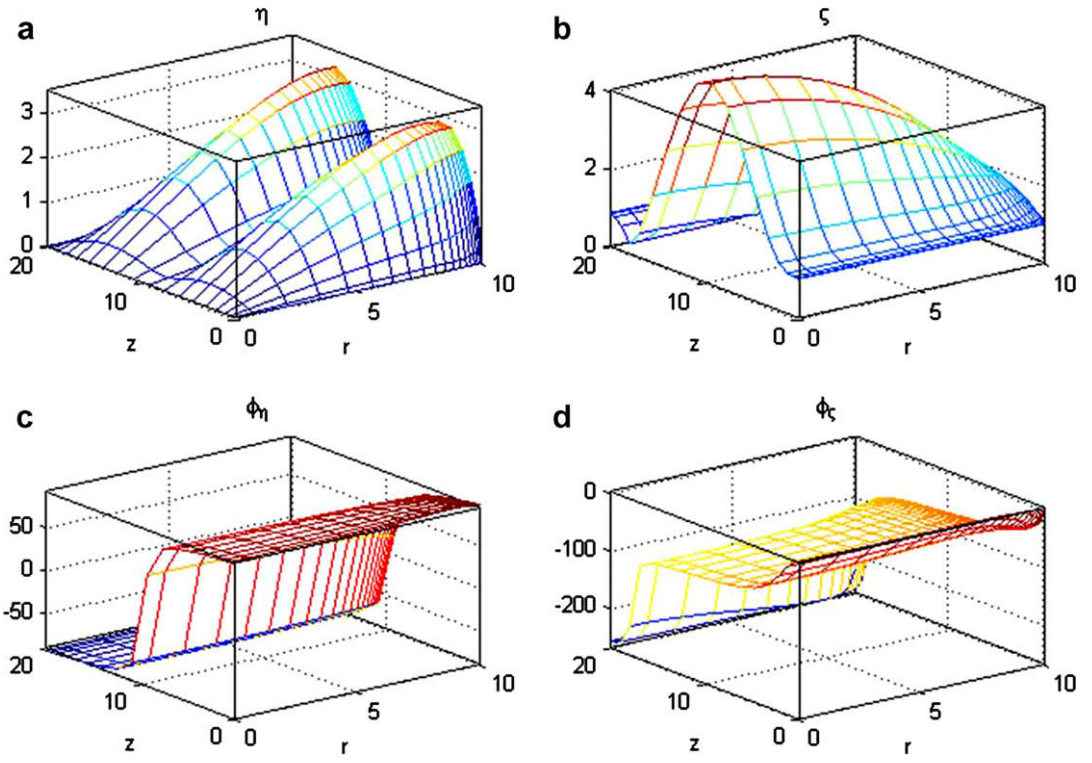

Fig. 4. Distribution of 2D deformation wave at fundamental resonance frequency $f = f_{\text{fund}}$; (a) amplitude of radial deformation η_0, (b) amplitude of axial deformation ζ_0, (c) phase of radial deformation φ_η, (d) phase of axial deformation φ_ζ.

$$\begin{matrix} E \\ \mu \end{matrix} \xrightarrow{\text{2Dmodel}} \begin{matrix} Z(f) \\ \theta(f) \end{matrix} \xrightarrow{\text{1Dmodel}} \begin{matrix} E_{\text{eff}}(f) \\ \mu_{\text{eff}}(f) \end{matrix} \tag{32}$$

Typical curves of the form factors α_E and α_μ for the range $0° < \theta < 140°$ are shown in Fig. 5 for several sets of the governing parameters. As seen, one-dimensional results overestimate E and underestimate μ. Meanwhile, the frequency behavior of the curves looks quite similar. Therefore, one can expect a frequency correction factor which depends on a single similarity variable.

The frequency correction factor $K(f)$ is searched in connection with the following relation

$$\alpha_E(f) = \frac{E}{E_{\text{eff}}(f)} = \frac{E}{E_{\text{eff}}(0)} \frac{E_{\text{eff}}(0)}{E_{\text{eff}}(f)} = \alpha_E(0) \frac{E_{\text{eff}}(0)}{E_{\text{eff}}(f)} = \frac{\alpha_E(0)}{K(f)},$$

where $\alpha_E(0)$ corresponds to the static form factor. This is because the static form factor is readily obtainable from simple analysis, which is shown in the Appendix. The frequency correction factor $K(f)$ and the form factor for loss

Table 1
Parameters of the samples for calculation of the form factor in normal mode.

E (MPa)	η	σ	H (cm)	R/H	ρ (g/cm^3)
0.5,1, 2	0.3	0.495	1	1	1
1	0.1, 0.3, 0.5	0.495	1	1	1
1	0.3	0.30, 0.40, 0.45, 0.495	1	1	1
1	0.3	0.495	0.5,1.0,1.5,2.0,3.0	1	1
1	0.3	0.495	1	1/4,1/3,1/2,1,2,3,4	1
1	0.3	0.495	1	1	1/8,1/4,1/2, 1,2,4,8

Table 2
Parameters of the samples for calculation of the form factor in shear mode.

E (MPa)	η	σ	R_0/H	R_1/R_0	H (cm)	ρ (g/cm^3)
0.5,1, 2	0.3	0.495	1	1	1	1
1	0.1,0.3, 0.5	0.495	1	1	1	1
1	0.3	0.30, 0.40, 0.45,0.495	1	1	1	1
1	0.3	0.495	1/4, 1/3, 1/2, 1, 2, 3, 4	1	1	1
1	0.3	0.495	1	1.25, 1.5, 2, 3, 5	1	1
1	0.3	0.495	1	1	0.5, 1.0, 1.5, 2, 3	1
1	0.3	0.495	1	1	1	1/8, 1/4, 1/2, 1, 2, 4, 8

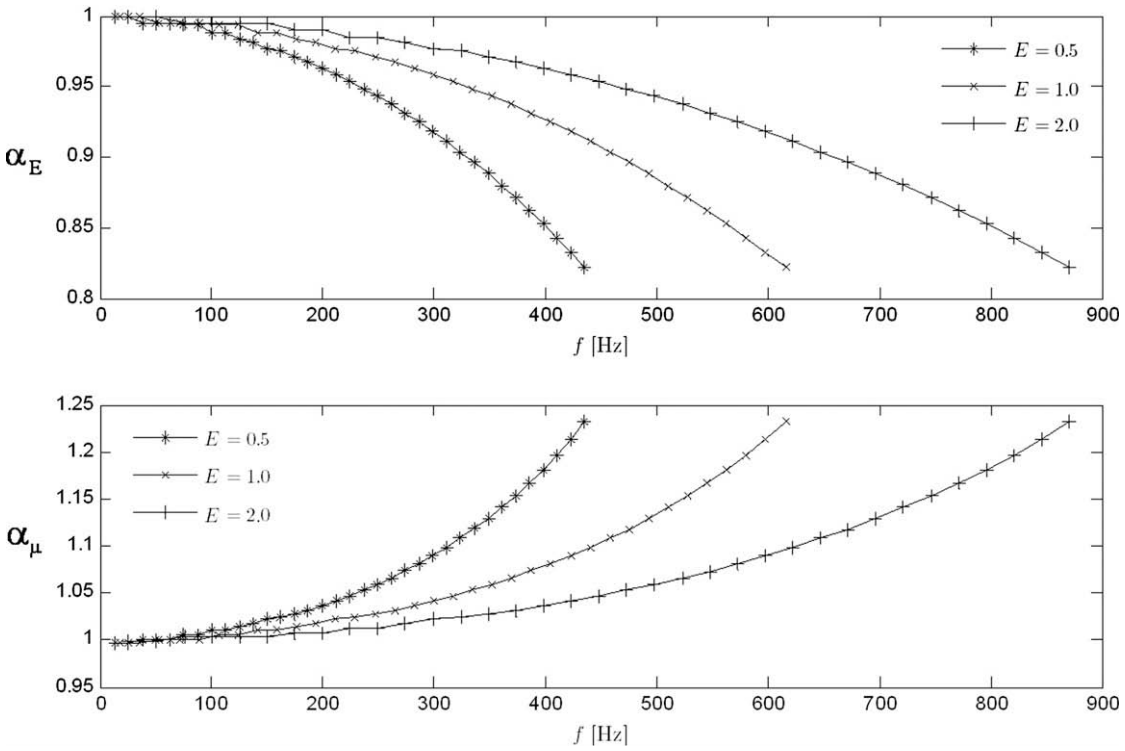

Fig. 5. Typical calculation result for the form factors for $E = 0.5$, 1.0, 2.0 MPa, $\mu = 0.3$, $\sigma = 0.495$, R =10 mm, $H = 20$ mm; (a) $\alpha_E(f) \equiv E/E_{\text{eff}}(f)$, (b) $\alpha_\mu(f) \equiv \mu/\mu_{\text{eff}}(f)$.

tangent for the whole 24 cases listed in Table 1 are plotted in Fig. 6. In the present study, normalization of the frequency has been attempted in terms of a generalized frequency defined as

$$F_{\text{stress}} = \frac{f}{f_{\text{fund}}} \frac{\sigma}{1-\sigma}\sqrt{\frac{R}{H}} \quad \left(f_{\text{fund}} = \frac{1}{2H}\sqrt{\frac{E}{\rho}}\right). \tag{33}$$

As seen, the collapse between different cases encompassing wide range of parameters E, ρ, σ, H, R/H is remarkably good. The curves of $K(F_{\text{stress}})$ and $\alpha_\mu(F_{\text{stress}})$ are virtually the same up to $\theta = 90°$ and for the range $90° < \theta < 140°$ the scatter between the curves does not exceed 5%.

It is notable that f_{fund} depends again on E, which is *a priori* unknown in real practice, if we use one-dimensional

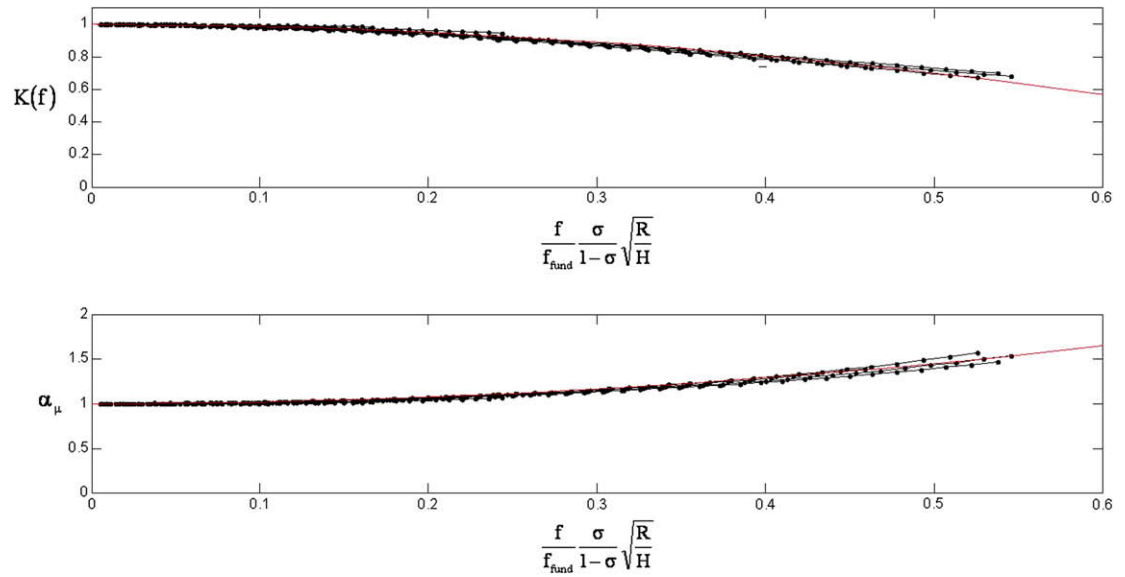

Fig. 6. Correction curves for E and μ versus generalized frequency (normal deformation mode).

calculation model. In this case, E_{eff} can be used instead to approximate f_{fund} and appropriate iteration procedures are to $\alpha_\mu(F_{\text{stress}}) = 1 + 1.8F^2_{\text{stress}}$be applied to improve the correction factors. We suggest the following empirical formulas of engineering interest, which approximate $K(F_{\text{stress}})$ and $\alpha_\mu(F_{\text{stress}})$;

$$K(F_{\text{stress}}) = 1 - 1.2F^2_{\text{stress}}. \quad (34)$$

$$\alpha_\mu(F_{\text{stress}}) = 1 + 1.8F^2_{\text{stress}} \quad (35)$$

The form factors for the case of dynamical shear deformation (Fig. 1b) α_G and α_μ were determined similarly. The parameters used for one- and two-dimensional calculations are listed in Table 2. These parameters are the same as those for the case of normal deformation plus those supplemented by the ratio R_1/R_0 in the range from 1.25 to 5.0. Fig. 7(a and b) demonstrates the results for in total of 28 parameter combinations. The results are presented in Fig. 7 against the frequency parameter $F_{\text{shear}} = \frac{f}{f_{\text{fund}}}$. Interestingly enough, the form factors for the shear mode are close to 1 for all frequencies under consideration and do not depend on Poisson's ratio and geometrical parameters of a sample.

The above results were obtained for a low frequency range near the parametric resonance frequency – the first maximum in the amplitude–frequency characteristic for the sample deformation, where phase changes from 0° to 180° (as shown in Fig. 2). Separate numerical tests showed similar behaviors of the form factors near the second resonance, where phases change from 180° to 360°.

4. Conclusions

Periodic axial as well as radial deformations of the cylinder and the annulus samples loaded by different masses, which are excited at frequency lower than the natural resonance ($\theta < 180°$), were investigated numerically by two-dimensional elastic wave equation. Obtained results were compared with those using the simplest one-dimensional model. It is shown that the dynamic form factor $\alpha_E(f)$ differ from the static analog $\alpha_E(0)$ only slightly. Dynamic form factor $\alpha_\mu(f)$ is also introduced. Empirical formulas of engineering interest for the correction factors $K(f)$ and $\alpha_\mu(f)$ are proposed in connection with generalized frequency. This is toward a correction of the simplest one-dimensional estimate of viscoelastic properties with an acceptable degree of accuracy in a wide parameter combination. The applicability range of the present method is also outlined. It is shown that in the setup for the shear measurements influence of sample dimensions can be disregarded for $f/f_{\text{fund}} < 0.4$. The static form factor $\alpha_E(0)$ was calculated using two-dimensional model of cylinder sample deformation and Hooke's law when the ratio of thickness to diameter changed from 0.1 to 10 and Poisson's

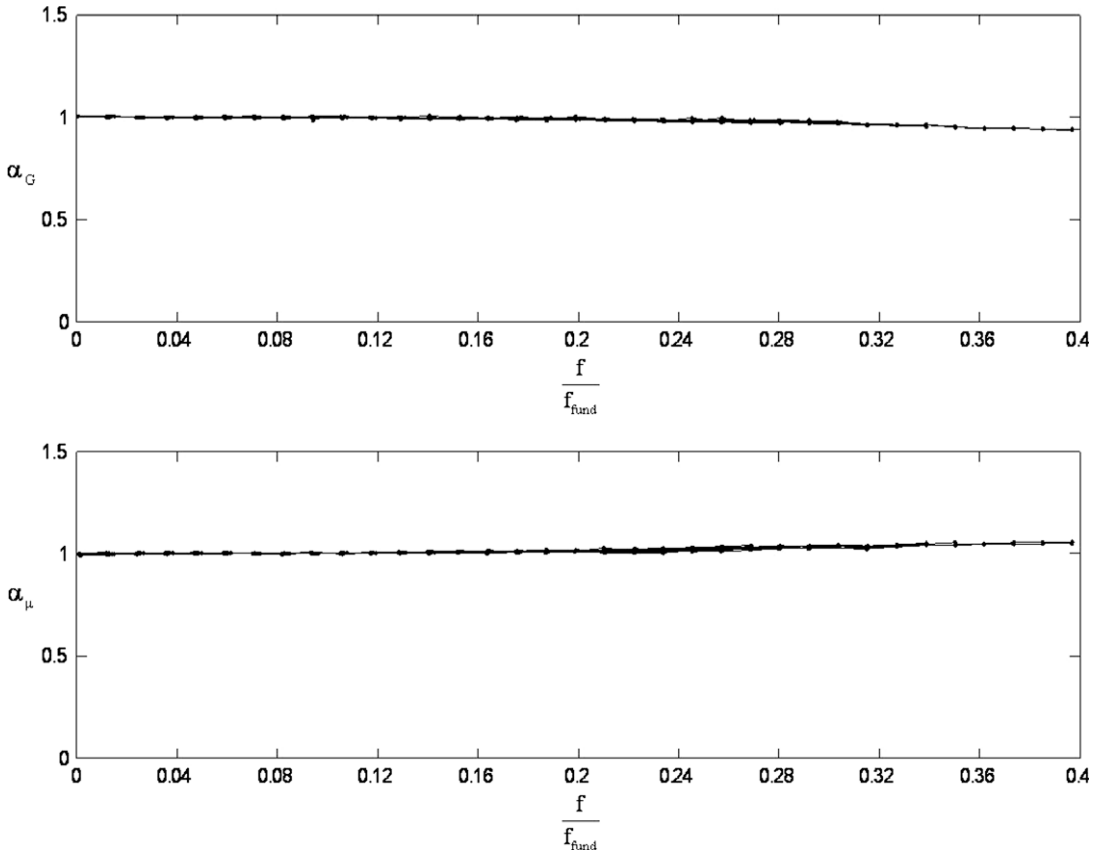

Fig. 7. Correction curves for G and μ versus generalized frequency (shear deformation mode).

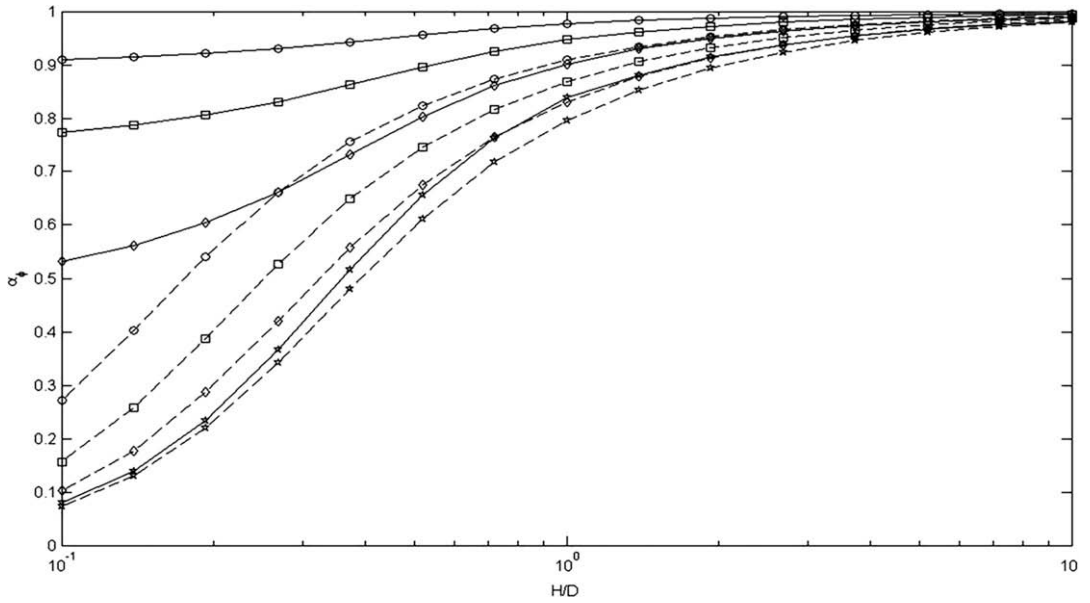

Fig. 8. Static form factor for Poisson's ratios: 0.2 (○), 0.3 (□), 0.4 (◇), 0.499 (∗) obtained by the numerical calculations (*solid lines*) and by an analytic technique (Rosin, 1972) (*dashed lines*).

ratio was varied from 0.2 to 0.499. For precise measurements in very wide region of experimental parameters it is necessary to use the 2D model of calculation of viscoelastic properties described in this paper.

Acknowledgements

This work was financially supported by Russian Foundation for Basic Research No. 06-08-00193-a and the ERC program (Advanced Ship Engineering Research Center) of MOST/KOSEF (Grant #: R11-2002-104-05001-0).

Appendix A. Calculation of static form factor

The technique described in Section 2.2 can be used also to calculate the static modulus of elasticity. In this case Eq. (1) takes the form (Landau and Lifschitz, 1986)

$$\Delta\vec{\xi} + \frac{\sigma}{1-2\sigma}\nabla(\nabla\cdot\vec{\xi}) = 0,$$

with the boundary conditions Eqs. (4)–(9), if we put $\omega = 0$ in Eqs. (6), (7). Instead of dynamic compatibility condition of Eq. (10), the balance of the load mass and internal deformations at the upper edge of the cylinder in the form is used

$$Mg = -\frac{2\pi E(1-\sigma)}{(1+\sigma)(1-2\sigma)}\int_0^R \frac{\partial\zeta}{\partial z}(H,r)rdr,$$

where E is real. In a typical experiment, the static deformation a as a function of varying load masses M is measured. The effective modulus of elasticity is defined by the Hook's law

$$E_{\text{eff}} = \frac{Mg}{\pi R^2}\frac{H}{a}.$$

Then, the static form factor is given by the ratio $\alpha = E/E_{\text{eff}}$.

Fig. 8 shows the form factors obtained by the numerical technique of present study and using an analytical formula

$$\alpha = 1 - K\tanh\frac{1}{K}, K = \frac{\sigma}{\sqrt{1+\sigma}}\frac{R}{H}.$$

obtained by a variational method for $\sigma \approx 0.5$ (Rosin, 1972). This indicates that at $\sigma \approx 0.5$ the numerical calculations provide form factor values close to those obtained analytically, while at smaller Poisson's ratios the analytical predictions underestimate α especially at $H/D < 1$.

References

Canuto, C., Hussaini, M.Y., Quarterony, A., Zang, T.A., 1988. Spectral methods in fluid dynamics. Springer Series in Computational Physics. Springer, Berlin.

Chen, C.P., Lakes, R.S., 1989. Apparatus for determining the viscoelastic properties of materials over ten decades of frequency and time. J. Rheol. 33 (8), 1231–1249.

Ferry, J.D., 1961. Viscoelastic Properties of Polymers, NY, London.

Fitzgerald, E.R., Ferry, J.D., 1953. Method for determining the dynamic mechanical behavior of gels and solids at audio-frequencies; comparison of mechanical and electrical properties. J. Colloid Sci. 8 (1), 1–34.

Fletcher, R., 1980. Practical Methods of Optimization, vol. 1. Unconstrained Optimization, John Wiley and Sons.

Grinchenko, V.T., Meleshko, G.L., 1981. Harmonic Oscillation and Waves in Elastic Bodies. Kiev, Naukova Dunka.

Kulik, V.M., Semenov, B.N., 1986. The two-parametric method for measurements of viscoelastic properties of polymer materials. Metrologiya 4, 32–38.

Kulik, V.M., Rodyakin, S.V., Lee, I., Chun, H.H., 2005. Deformation of a viscoelastic coating under the action of convective pressure fluctuations. Exp. Fluids 38 (5), 648–655.

Kulik, V.M., Semenov, B.N., Morosova, S.L., 2007. Measurement of dynamic properties of viscoelastic materials. Thermophysics and Aeromechanics 14 (2), 219–230.

Kulik, V.M., Semenov, B.N., Boiko, A.V., Seoudi, B.M., Chun, H.H., Lee, I., 2008. Measurement of dynamic properties of viscoelastic materials. Exp. Mech. doi: 10.1007/s11340-008-9165-x.

Landau, L.D., Lifschitz, E.M., 1986. Theory of Elasticity, third ed. Pergamon Press, Oxford, England.
Madigosky, W.M., Lee, G.F., 1983. Improved resonance technique for materials characterization. J. Acoust. Soc. Am. 73, 1374–1377.
Riande, E., Diaz-Calleja, R., Prolongo, M.G., Masegosa, R.M., Salom, C., 2000. Polymer viscoelasticity. Stress and strain in practice. Marcel Dekker Inc., New York, Basel.
Rosin, G.S., 1972. Measurement of dynamic properties of acoustic materials. Stroyizdat, Moskow.
Sadd, H.M., 2005. Elasticity. Theory, Applications, and Numerics. Elsevier Inc.
Smith, G.M., Beirman, R.L., Zitek, S.J., 1983. Determination of dynamic properties of elastomers over broad frequency range. Exp. Mech. 23 (2), 158–164.
Tang, T., Trummer, M.R., 1996. Boundary layer resolving pseudospectral methods for singular perturbation problems. SIAM J. Sci. Comp. 17 (2), 430–438.
Timoshenko, S.P., Groodier, J.N., 1982. Theory of Elasticity. McGraw-Hill, London.
Trefethen, L.N., 1990. Approximation theory and numerical linear algebra. In: Mason, J., Cox, M. (Eds.), Algorithms for Approximation II. Chapman and Hall, London, pp. 336–361.
Tsai, H.-C., Hsueh, S.-J., 2001. Mechanical properties of isolation bearing identified by a viscoelastic method. Solids Struct. 38, 53–74.
Tsai, H.H., 2005. Compression analysis of rectangular elastic layers bonded between rigid plates. Solids Struct. 42, 3395–3410.